Accurate capture of rudder-propeller interaction using a coupled blade element momentum-RANS approach

Alexander Phillips*, Maaten Furlong and Stephen R Turnock***

*Fluid-Structure Interaction Research Group, School of Engineering Sciences, University of Southampton, Highfield, Southampton SO17 1BJ, UK

**National Oceanography Centre, Southampton, European Way, Southampton, SO14 3ZH, UK

Corresponding author's email: abp@soton.ac.uk

1 Introduction

Ship rudders are almost always placed downstream of the propeller so they can take advantage of the increased local velocity due to the presence of the propeller race. The methods discussed in this paper replicate the flow integrated effects of the propeller which generates an accelerated and swirled onset flow onto the rudder. As long as the radial variation in axial and tangential momentum (including hull and rudder interaction effects) generated by the propeller are included, then the influence of the unsteady propeller flow can be removed and 'steady' calculations performed to evaluate propeller rudder interaction.

Three different body force propeller models will be considered and numerical results will be compared with experiments by Molland and Turnock [1, 2, 3], using the modified Wageningen B4.40 propeller and Rudder No.2.

2 Theoretical Approach

The flow around a rotating propeller is a highly complex 3D transient flow, therefore modelling a rotating propeller explicitly leads to significant computational cost within a RANS simulation. This is due to the high mesh resolution required around the blade to capture the flow features and the small time steps required to capture the transients flow features. For work not concentrating on the propeller itself but rather the interaction of the propeller hull and rudder system it may not be vital to capture all aspects of the propeller flow, however providing a representative model of the velocity field is extremely important. Based on this assumption several body force propeller models have been proposed to reduce computational cost, which facilitate self propelled simulations.

When using a body force model the propeller is not physically represented by its geometry. Instead the effect of the propeller on the flow is included by representing the propeller as a series of axial and momentum source terms, fb_x and fb_θ respectively, which are distributed over the propeller disc, these induce an axial and swirl acceleration in the fluid.

In order to implement a body force propeller model in a RANS simulation both the magnitude and distribution of the thrust, T, and torque, Q, induced by the propeller needs to be determined. Three different bodyforce models will be considered:-

1. Uniform thrust distribution with no torque, equivalent to an actuator disc applied over a finite thickness.
2. Hough and Ordway prescribed thrust and torque distribution.
3. Thrust and torque magnitude and distribution from Blade Element Momentum Theory (BEMT).

Typical velocity profiles available in the literature, [4], show that the velocity in the radial direction is an order of magnitude smaller than the tangential velocity component, hence it is assumed valid to not model the blade local induced radial velocity changes. Radial velocity changes due to contraction of the slipstream are incorporated by the RANS equations in order to maintain continuity.

2.1 Uniform Thrust Distribution - RANS-UT

A uniform distribution of thrust is assumed and the torque is neglected, equivalent to momentum theory. The axial momentum source term is given by:-

$$fb_x = \frac{T}{\Delta x \pi (R_p^2 - R_h^2)}, \tag{1}$$

while the tangential momentum term is given by:-

$$fb_\theta = 0, \tag{2}$$

where Δx is the thickness of the propeller subdomain and R_h and R_p are the radius of the hub and propeller respectfully. The magnitude of T must be provided by some other means, either experimental, based on open water data or from numerical predictions.

2.2 Hough and Ordway Thrust and Torque Distribution - RANS-HO

The radial distribution of thrust and torque is based on the [5] circulation distribution which has zero loading on the tip and root. The distribution was shown to closely match Goldstein's optimum distribution. Coupling this distribution with a RANS simulation was proposed by [6], and is implemented in CFDSHIP-IOWA, [7]. The non-dimensional thrust distribution fb'_x and torque distribution fb'_θ are given by:-

$$fb'_x = A_x r^* \sqrt{1 - r^*} \tag{3}$$

$$fb'_\theta = A_\theta \frac{r^*\sqrt{1-r^*}}{(1-Y_h)r^* + Y_h} \tag{4}$$

Where:

$$A_x = \frac{C_T}{\Delta x} \frac{105}{16(4+3Y_h)(1-Y_h)} \tag{5}$$

$$A_\theta = \frac{K_Q}{\Delta x J^2} . \frac{105}{\pi(4+3Y_h)(1-Y_h)} \tag{6}$$

where the non dimensional radius is defined as $r^* = (Y - Y_h)/(1 - Y_h)$, $Y = r/R_p$ and $Y_h = R_h/R_p$.

$$C_T = \frac{T}{1/2\rho U_a^2 \pi R_p^2} = \frac{K_T}{\pi/8J^2} \tag{7}$$

For uniform propeller inflow such as that experienced by a propeller rudder system operating in freestream, [8] demonstrated that the use of this thrust and torque distribution lead to good estimates of rudder forces.

2.3 Blade Element Momentum Theory, Thrust and Torque Magnitude and Distribution Prediction - RANS-BEMT

The thrust and torque distribution will vary depending on the geometry of the propeller, rpm and advance velocity. To incorporate these variations the thrust and torque magnitude and distribution are calculated using an existing Blade Element Momentum Theory code [9].

In order to capture the radial and circumferential variation in propeller inflow conditions due to blockage effects from the rudder, the propeller plane is subdivided into for 360 discrete zones (10 radial divisions, 36 circumferential divisions). The BEMT code is called for each of these locations to determine the local K_T and K_Q based on local inflow conditions. For each node in the propeller subdomain, the radial distance is calculated and the local thrust and torque magnitudes are interpolated from the distribution derived from the BEMT code. Further details of this approach may be found in [10, 11, 12].

3 Experimental Data

Wind tunnel tests performed by Molland and Turnock in the University of Southampton $3.5 \times 2.5m$ RJ Mitchell Wind Tunnel [13]. The experimental set up is shown in Figure 1, it comprises of a 1m span, 1.5 geometric aspect ratio rectangular planform rudder, and a representative 0.8m diameter propeller based on the Wageningen B4.40 series placed at $X/D = 0.39$. Further details of the experiment can be found in [3].

4 Numerical Model

The motion of the fluid is modelled using the incompressible (8), isothermal Reynolds Averaged Navier Stokes (RANS) equations (9) in order to determine the cartesian flow field $(u_i = u, v, w)$ and pressure (p) of the water around the hull:

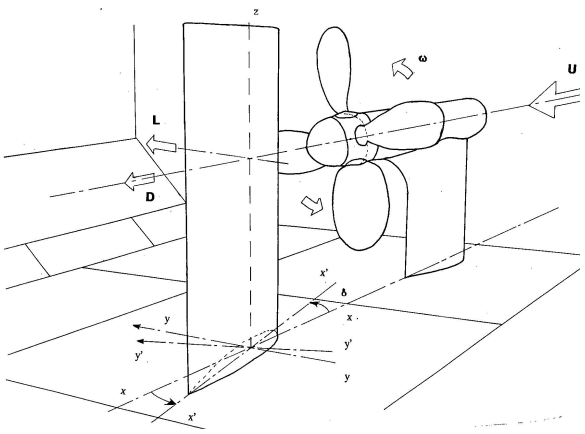

Figure 1: Isometric view of experimental setup, [1]

$$\frac{\partial \overline{U_i}}{\partial x_i} = 0 \tag{8}$$

$$\rho \frac{\partial \overline{U_i}}{\partial t} + \rho \frac{\partial \overline{U_i U_j}}{\partial x_j} = -\frac{\partial P}{\partial x_i} + \frac{\partial}{\partial x_j} \left\{ \mu \left(\frac{\partial \overline{U_i}}{\partial x_j} + \frac{\partial \overline{U_j}}{\partial x_i} \right) \right\} - \rho \frac{\partial \overline{u_i' u_j'}}{\partial x_j} + f_i \tag{9}$$

The influence of turbulence on the mean flow is represented in equation (9) by the Reynolds stress tensor $(\rho \overline{u_i' u_j'})$.

Closure of the RANS equations is achieved for this case using the Shear Stress Transport (SST) model eddy viscosity turbulence closure model developed by [14]. SST is a two zone model that blends a variant of the $k-\omega$ model in the inner boundary layer with a transformed version of the $k-\varepsilon$ in the outer boundary layer and away from the wall. Previous investigations for Ship flows have shown it is better able to replicate the flow around ship hull forms than either zero equation models or the $k-\varepsilon$ model, notably in capturing hooks in the wake contours at the propeller plane, [15].

Simulations are performed using ANSYS CFX, a commercial, fully implicit finite volume code, using a variation of the SIMPLE (Semi-Implicit Method for Pressure Linked Equations) algorithm for momentum-pressure decoupling. Details of the computational model are provided in Table 1.

4.1 Model Domain and Boundary Conditions

The lateral dimensions were matched to those of the RJ Mitchell wind tunnel, with the domain extending 2.8 chord lengths upstream of the rudder and 8 chord lengths downstream. The following boundary conditions were applied:

- Inlet - Dirchlet boundary condition, nominal inflow velocity 10 m/s, with representative 70mm thick boundary layer distribution applied over floor, turbulence intensity 0.002, eddy length scale 0.01m.
- Outlet - Neumann boundary condition, velocity and pressure gradients set to zero, with a zero relative pressure

Table 1: Computational model

Parameter	Setting
Mesh Type	Unstructured with local refinement in vortical regions
No. of Elements	approximately 10M
Computing	Iridis 2 Linux Cluster
Run Type	Parallel (8 partitions run on 4×dual core nodes each with 2Gb RAM)
Turbulence Model	Shear Stress Transport
y^+	30-60 on rudder, 200 on floor
Wall Modelling	Automatic Wall Functions
Spatial Discretisation	High Resolution
Pseudo Time Step	0.1s
Convergence Control	RMS residual $< 10^{-5}$
Simulation Time	Typically 2.5-3hrs

- Floor - no slip, initial studies neglecting the floor boundary layer were unable to replicate the flow at the root of the rudder.
- Walls - free slip
- Rudder - no Slip
- Hub - no Slip

Within the RANS simulation the propeller is modelled as a cylindrical subdomain with a diameter equal to that of the propeller and a length equal to that of the rotating hub. Momentum source terms are then applied over the subdomain in cylindrical co-ordinates to represent the axial and tangential momentum induced by the propeller, as calculated by the three body force propeller models.

5 Flow Feature Identification and Mesh Refinement

The structure of the flow downstream of a rudder operating in freestream conditions is well understood. However the influence of the propeller upstream results in a highly complex flow, the tip vortex generated by the rudder acts to break up the propeller race. Since the race itself incorporates a large swirl component as the wake is broken up it has a tendency to roll up into a series of secondary vortices. The number and path of which is impossible to predict *a priori*.

To track these vortex structures the VORTFIND algorithm [16] is used. The VORTFIND algorithm is a robust and computationally inexpensive method of identifying the vortex core centre using just the velocity data on a transverse plane, and is extended to three dimensions through using a series of planes that are normal to the local vortex direction, [17].It is a line method, that is not Galilean invariant but allows multiple vortices to be captured, only requiring knowledge of the velocity field. The original VORTFIND algorithm has been successfully used to identify bilge vortices, control surface tip vortices and propeller tip vortices. Modifications to the algorithm to make it more robust when identifying multiple vortex structures are detailed in [18].

In order to ensure suitable spatial resolution of the vortex structures an iterative unstructured mesh strategy is used.

1. An initial coarse mesh is produced with approximately 100000 elements in the propeller domain and 1.5 million elements in the far field. A separate mesh is built for each rudder angle, which is used for the three different propeller model approaches.

   The resulting flow field contains diffuse flow features but enables regions of interest to be identified. At a series of tangential cut planes downstream of the the rudder the lateral and vertical extents of the propeller race are identified. The extent of the propeller race is determined as the location where $u/U_0 > 1.0$.

2. TCL scripts then take the extents of the wake and enter this data into ICEM CFD as a series of mesh density regions. A second finer mesh is built with an approximate far field mesh size of 4.0M elements.

   Since the extent of the propeller race are different for each of the three propeller models a different mesh must be built for each case.

   Since the preliminary coarse mesh has insufficient elements to capture the flow features downstream of the rudder, to a suitable level of precision, insufficient elements leads to numerical diffusion of the features resulting in weaker larger structures than a mesh resolved solution. By placing more elements in the region of the propeller race, a better estimate of the extent of these flow features can now be achieved.

3. The results from these secondary meshes are examined more closely, the rudder tip vortex and secondary vortex structures are identified using the modified Vortfind algorithm.

4. Finally a final fine mesh is built placing finer mesh in the regions of the propeller race, tip vortex (the tip vortex is assumed to originate at 2/3rd chord at the junction between the tip and pressure surfaces), secondary vortices and rudder boundary layer.

Figure 2 at the rear of the paper illustrates the downstream mesh refinement process. The initial coarse mesh results in highly diffused flow structures. The tip vortex is evident in the lateral vector plot but none of the secondary vortices have propagated this far downstream X/D=7.0. However the initial mesh provides a good first estimate of the extents of the propeller race.

6 Results and Discussion

Preliminary results are presented below for a propeller operating condition of $J = 0.35$, further smoothing of the mesh is required in the mesh transition region between the floor boundary layer and rudder boundary layer. Some poor quality elements in this region are leading to numerical instabilities, visible in the rudder surface pressure plots.

6.1 Lift and Drag Data

Figure 3 and 4 compares the experimental and numerical lift and drag respectively. Results are also presented from [8] who performed similar numerical simulations using the CFDSHIP-IOWA code using a Hough and Ordway thrust and torque distribution, and from [19] using the 3D panel code Palisupan, [20]. Table 2 compares values of $dC_L/d\delta$ and δ_0.

By neglecting the influence of propeller induced swirl on the fluid, the RANS-UT model produces symmetric results at $\pm 10°$ and the rudder neutral angle is at $0°$. However the magnitude of the lift results provide good indicative results, the gradient of the lift slope is within 10% of mean experimental value. For this case the drag experienced by the rudder is significantly greater than the experimental results for the RANS-UT model, this is due to the influence of swirl on local incidence angle. Experimental results show a decrease in rudder drag with increasing propeller thrust loading.

The RANS-HO and RANS-BEMT approaches show very good correlation with the experiential lift results in terms of both neutral rudder angle, δ_0, and lift slope gradient. The asymmetry due to the swirl action of the propeller is well reproduced.

Table 2: Propeller details

Data Set	$\frac{dCL}{d\delta}$	δ_0
Molland and Turnock SS46	0.132	0.093
Molland and Turnock SS90	0.136	0.526
Turnock (1993)	0.140	1.376
Simonseen 2000	0.147	1.383
RANS-UT	0.124	0.000
RANS-HO	0.136	0.255
RANS-BEMT	0.142	0.264

6.2 Rudder Surface Pressure

The ability of the three propeller models to replicate the downstream wake of a propeller can be inferred by their ability to replicate the correct pressure distribution on the rudder surface.

Examining the $C_P = \frac{P-P_0}{1/2\rho U_0^2}$ distribution for a freestream rudder, you observe a C_P value of 1.0 at the stagnation point, where the flow velocity drops to zero. For a rudder downstream of a propeller the inflow velocity is greater than the freestream velocity, hence the stagnation pressure is higher leading to C_P

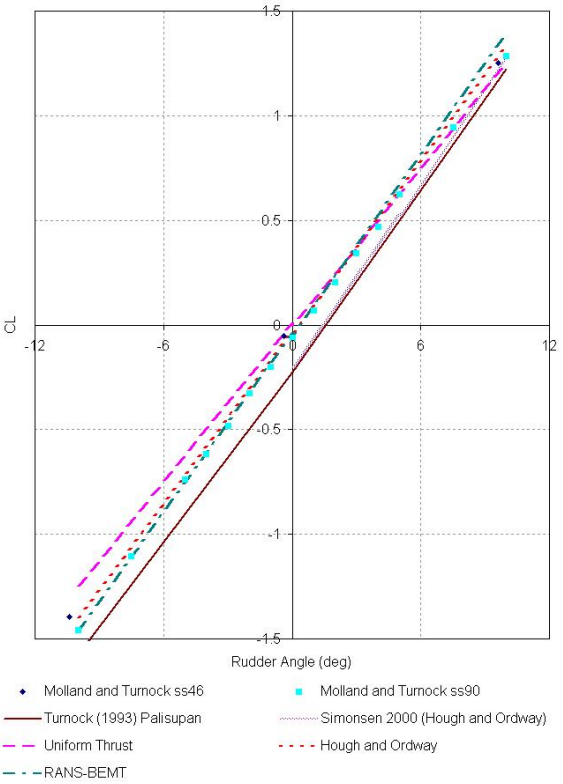

Figure 3: Rudder 2 - CL performance J=0.35

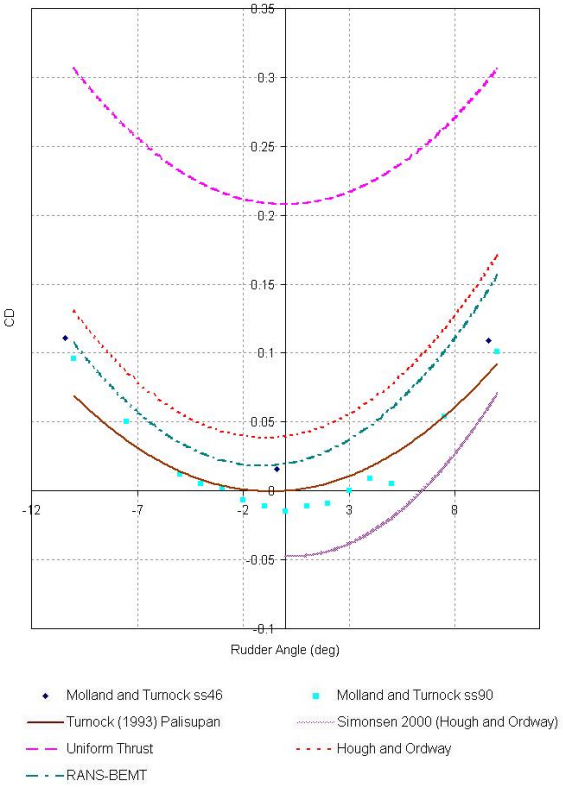

Figure 4: Rudder 2 - CD performance J=0.35

values in excess of 1. Accurate prediction of stagnation c_P values implies the correct inflow velocity has been generated by the propeller model.

Figure 5 compares experimental and numerical pressure distributions at a series of span locations from root to tip for a rudder angle of $\delta = 0$.

The RANS-UT model experiences a symmetric pressure distribution down both sides of the rudder in stark contrast to the more complex models and the experimental data. Both the RANS-BEMT and RANS-HO models relatively well reproduce the pressure distribution for most of the locations considered showing clear improvement over the RANS-UT approach.

Both the RANS-BEMT and RANS-HO approaches are relatively well able to replicate the pressure distribution at incidence angles of both 10 and -10 degrees. Since the swirl imparted swirl direction is constant in both cases the resulting pressure fields are substantially different and this is reproduced in the numerical results.

7 Conclusions

The methods discussed in this paper make use of the flow integrated effects of the propeller which generates an accelerated and swirled onset flow onto the rudder. As long as the radial variation in axial and tangential momentum generated by the propeller are included, then the influence of the unsteady propeller flow can be removed and 'steady' calculations performed to evaluate the influence of the propeller on the rudder.

The uniform thrust approach which neglects swirl results in adequate prediction of rudder lift but is unable to well predict the rudder drag.

The prescribed thrust and torque distribution of Hough and Ordway and the coupled RANS-BEMT approach are better able to recreate the wake downstream of the propeller and the resulting rudder loads and surface pressure distribution compare favourably with the experimental data.

This RANS-HO approach is only useful to investigate the influence of the propeller on the rudder. Interaction effects due to the rudder on the propeller are not captured, and neither would the influence of the hull on the propeller inflow conditions. The blockage effects of the rudder or influence of non uniform inflow into the propeller can be achieved using the coupled RANS-BEMT approach described, making it more suitable for cases involving hull, propeller and rudder such as self propulsion simulations.

Acknowledgements

Mr Phillips' PhD studentship is jointly financed by the School of Engineering Science and the National Oceanography Centre, Southampton.

References

[1] A. F. Molland and S. R. Turnock. Wind tunnel investigation of the influence of propeller loading on ship rudder performance. Technical report, Ship Science Report No. 46, 1991.

[2] A.F. Molland and S.R. Turnock. Wind tunnel tests on the effect of a ship hull on rudder-propeller performance at different drift angles. Technical report, University of Southampton Ship Science Report No. 76, May 1995.

[3] A.F. Molland and S.R. Turnock. *Marine Rudders and Control Surfaces*. Butterworth-Heinemann, 2007.

[4] C. Kee, G.A. Hamill, W-H. Lam, and P.W. Wilson. Investigation of the velocity distributions within a ships propeller wash. In *Proceedings of the Sixteenth (2006) International Offshore and Polar Engineering Conference San Francisco, California, USA,*, May 28-June 2, 2006.

[5] G. R. Hough and D. E. Ordway. The generalised actuator disc. *Developments in Theoretical and Applied Mechanics*, 2:317–336, 1965.

[6] F. Stern, H. T. Kim, N. M. Patel, and H. C. Chen. A viscous-flow approach to the computation of propeller-hull interaction. *Journal of Ship Research*, 32:246–262, 1988.

[7] E. G. Paterson, R.V. Wlison, and F. Stern. General purpose parrallel unsteady rans ship hydrodynamics code CFDSHIP-IOWA. Technical report, Iowa Institute of Hydraulic Research, The University of Iowa, 2003.

[8] C. D. Simonsen. *Rudder, Propeller and Hull Interaction by RANS*. PhD thesis, Department of Naval Architecture and Offshore Engineering, 2000.

[9] A. F. Molland and S. R. Turnock. A compact computational method for predicting forces on a rudder in a propeller slipstream. In *Transactions of RINA*, volume 138, pages 59–71, 1996.

[10] S.R Turnock, A.B. Phillips, and M Furlong. Urans simulations of static drift and dynamic manoeuvres of the kvlcc2 tanker. In *SIMMAN International Manoeuvring Workshop, Copenhagen*, April 2008.

[11] A.B. Phillips, M. Furlong, and S.R. Turnock. Comparisons of cfd simulations and in-service data for the self propelled performance of an autonomous underwater vehicle. In *27th Symposium on Naval Hydrodynamics Seoul, Korea*, 5-10 October 2008.

[12] A.B. Phillips, S.R Turnock, and M. Furlong. Simulation of a self-propelled ship using a blade element momentum propeller model and rans. *Submitted to Journal of Ocean Engineering*, 2009.

[13] WWW1. *http : //www.windtunnel.soton.ac.uk/index.html*. World Wide Web, 2009.

[14] F.R. Menter. Two-equation eddy-viscosity turbulence models for engineering applications. *AIAA Journal*, 32(8):1598 – 605, 1994.

[15] L. Larsson, F. Stern, and V. Bertram. Benchmarking of computational fluid dynamics for ship flows: The gothenburg 2000 workshop. *Journal of Ship Rese*, 47:63–81(19), 1 March 2003.

[16] R. J. Pemberton, S. R. Turnock, T. J. Dodd, and E. Rogers. A novel method for identifying vortical structures. *Journal of Fluids and Structures*, 16:1051–1057, 2002.

[17] C. Pashias. *PROPELLER TIP VORTEX SIMULATION USING ADAPTIVE GRID REFINEMENT BASED ON FLOW FEATURE IDENTIFICATION*. PhD thesis, University of Southampton, 2005.

[18] A. B. Phillips. *Cost effective hydrodynamic design of Autonomous Underwater Vehicles*. PhD thesis, School of Engineering Sciences, University of Southampton, to be submitted 2009.

[19] S.R. Turnock. *Prediction of ship rudder-propeller interaction using parallel computations and wind tunnel measurements*. PhD thesis, University of Southampton, Ship Science, 1993.

[20] S.R. Turnock. Technical manual and user guide for the surface panel code: Palisupan. Technical report, University of Southampton, Southampton, UK (Ship Science Reports, 100), 1997.

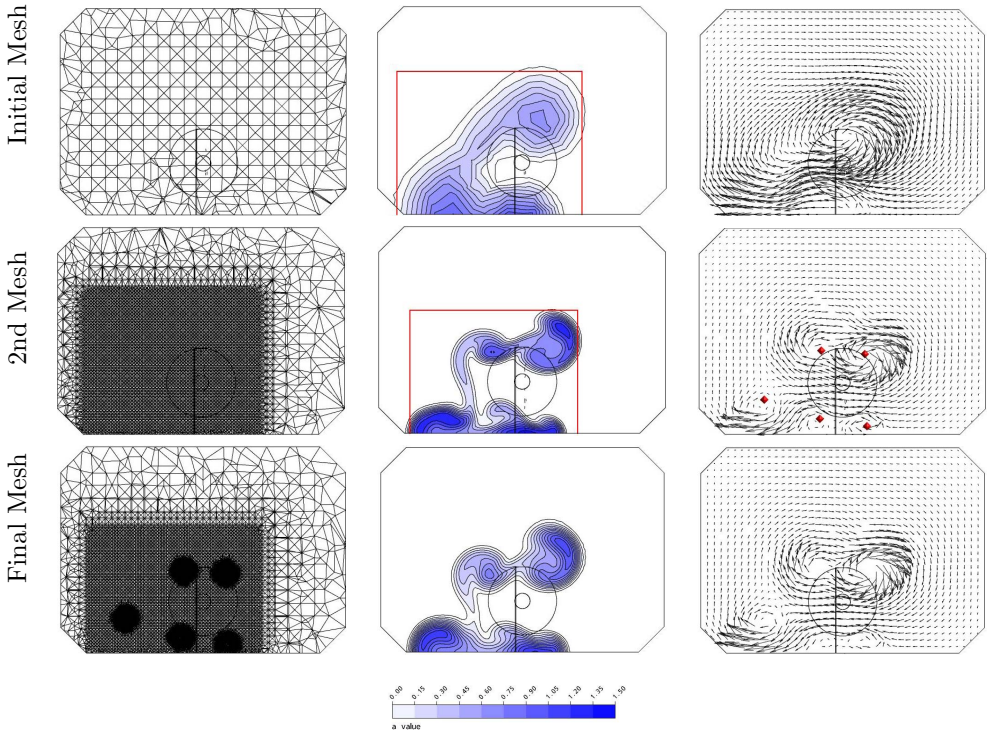

Figure 2: Example Downstream Mesh Strategy. Case - Hough and Ordway rudder at 10° incidence, J=0.35 X=1.6m. Mesh *(left)*, axial flow factor (*centre*) and transverse velocity vectors *(right)*. Vortex locations identified by the Vortfind V2 algorithm marked by red diamonds and the red box describes the lateral and vertical extents of the propeller race. This information is then used to help define refinement regions for the proceeding mesh

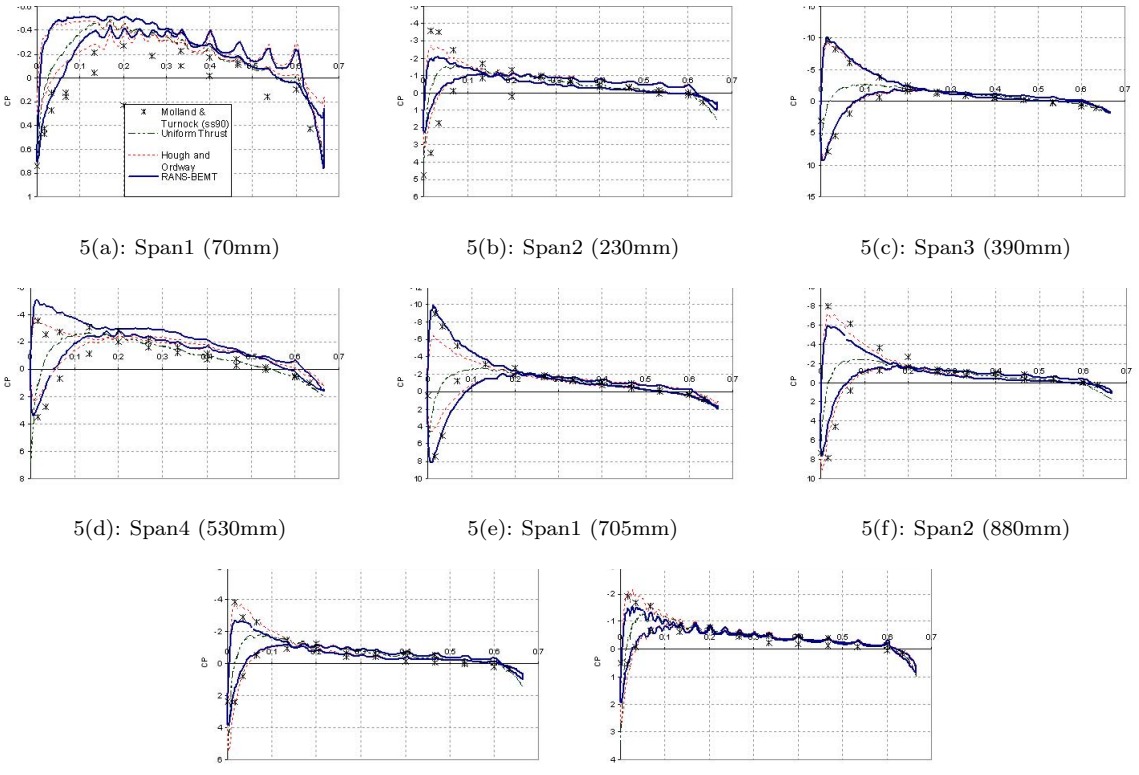

5(a): Span1 (70mm) 5(b): Span2 (230mm) 5(c): Span3 (390mm)

5(d): Span4 (530mm) 5(e): Span1 (705mm) 5(f): Span2 (880mm)

5(g): Span3 (940mm) 5(h): Span4 (970mm)

Figure 5: Rudder Pressure Distributions at 0° incidence